Appl. Phys. B 89, 311–318 (2007)
DOI: 10.1007/s00340-007-2815-3

Applied Physics B
Lasers and Optics

J.D.B. BRADLEY✉
F. AY
K. WÖRHOFF
M. POLLNAU

Fabrication of low-loss channel waveguides in Al_2O_3 and Y_2O_3 layers by inductively coupled plasma reactive ion etching

Integrated Optical MicroSystems (IOMS) Group, MESA+ Institute of Nanotechnology,
University of Twente, P.O. Box 217, 7500 AE Enschede, The Netherlands

Received: 22 June 2007/Revised version: 23 August 2007
Published online: 21 October 2007 • © Springer-Verlag 2007

ABSTRACT Etching of amorphous Al_2O_3 and polycrystalline Y_2O_3 films has been investigated using an inductively coupled reactive ion etch system. The etch behaviour has been studied by applying various common process gases and combinations of these gases, including CF_4/O_2, BCl_3, BCl_3/HBr, Cl_2, Cl_2/Ar and Ar. The observed etch rates of Al_2O_3 films were much higher than Y_2O_3 for all process gases except for Ar, indicating a much stronger chemical etching component for the Al_2O_3 layers. Based on analysis of the film etch rates and an investigation of the selectivity and patterning feasibility of possible mask materials, optimized optical channel-waveguide structures were fabricated in both materials. In Al_2O_3, channel waveguides were fabricated with BCl_3/HBr plasma and using a standard resist mask, while in Y_2O_3, channel waveguides were fabricated with Ar and using either a resist or a sputter deposited Al_2O_3 mask layer. The etched structures in both materials exhibit straight sidewalls with minimal roughness and sufficient etch depths (up to 530 nm for Al_2O_3 and 250 nm for Y_2O_3) for defining waveguides with strong optical confinement. Using the developed etch processes, low additional optical propagation losses (on the order of 0.1 dB/cm) were demonstrated in single-mode ridge waveguides in both Al_2O_3 and Y_2O_3 layers at 1550 nm.

PACS 42.70.-a; 42.82.-m; 42.82.Cr

1 Introduction

Aluminium oxide and yttrium oxide layers are known to be excellent hosts for rare-earth ions and prospective materials for active integrated optical applications [1]. Both materials have sufficiently large refractive indices for the realization of highly compact integrated optical devices and possess a high transparency, which is a prerequisite for low-loss optical waveguides. Moreover, they can be deposited on silicon substrates enabling compatibility with standard silicon technology. In particular, amorphous and polycrystalline Al_2O_3:Er [2] and polycrystalline Y_2O_3:Er [3] layers have been studied for laser and amplifier applications operating in the third telecommunications window (around 1550 nm). Each material offers different advantages, depending on the particular application: Al_2O_3:Er devices offer a broad emission line width, useful for amplification over a wide wavelength range and tuneable laser applications, while Y_2O_3:Er has a much narrower line width and higher peak cross sections, hence lower gain threshold, and higher thermal conductivity, all useful for single-wavelength laser applications. Due to these well-known advantages, the deposition of high optical quality rare-earth-ion-doped films of both Al_2O_3 and Y_2O_3 has recently been the subject of intense study [4–9]. Y_2O_3 films with losses of less than 1 dB/cm at 800 nm [10] have been demonstrated, and more recently as-deposited films with losses as low as 0.11 dB/cm at 1522 nm [11] have been demonstrated in Al_2O_3, showing the potential for low intrinsic waveguide losses, which are necessary for sufficient net gain in the doped layers.

In order to realize high-quality integrated active waveguide devices in such low-loss Al_2O_3 and Y_2O_3 layers, a reliable patterning technique is required. For Al_2O_3:Er, Ar-ion-beam milling (or sputtering) has previously been used to define ridge waveguide structures [12], and recently wet chemical etching has also been employed [13]. Y_2O_3 ridge waveguides have also been fabricated using Ar-beam sputtering [14] and wet chemical etching [15]. However, both techniques (physical etching via Ar-ion-beam milling and wet chemical etching) limit both the overall resolution of the process and the steepness of the sidewall profile. Furthermore, the etch depths were limited to 300 nm in the Ar milling case and less than 400 nm for wet etching of Al_2O_3. The structures obtained using Ar-ion-beam etching in Y_2O_3 were limited to 2-μm widths and only very shallow etch depths (< 100 nm) were reported.

With the aim of achieving sufficient gain in active waveguide devices, a fabrication technique is required with high resolution, sufficient etch depth and low additional losses introduced by the etch process itself. For high resolution, good selectivity to the mask material and steep (anisotropically etched) sidewalls are required. Deeply etched channels (as opposed to shallow-etched ridge-type structures) also may be required for high confinement to achieve good overlap of

✉ Fax: +31-53-489-3343, E-mail: j.d.b.bradley@ewi.utwente.nl

the pump and signal beams and minimize the bend radius (without significantly adding to the losses). Finally, for low additional losses due to channel etching, smooth sidewalls are required. Reactive ion etching (RIE) is the preferred etching method to achieve these goals, because it combines both physical and chemical etching mechanisms, resulting in optimized structures with steep, smooth sidewalls. The plasma etching characteristics of Al_2O_3 films in various chemistries have been widely studied [16–21], and recently reports on the RIE behaviour of Y_2O_3 films have also appeared in the literature [22, 23]. RIE of optical waveguides in Al_2O_3 films has been reported [24], but the process involved a complicated three-level masking procedure and utilized a metallic Cr mask, which is less desirable than other materials, because metals can introduce extra losses in the waveguide. In this paper, the etching behaviour of amorphous Al_2O_3 films, polycrystalline Y_2O_3 films, and possible masking materials are investigated using an inductively coupled plasma (ICP) RIE system. Based on the etching data, optimized processes have been developed for fabricating high-quality, low-loss channel waveguides in both materials. The optical propagation losses of the obtained channel waveguide structures have been characterized.

2 Experimental

Amorphous Al_2O_3 and polycrystalline Y_2O_3 films were reactively co-sputtered on thermally oxidized ⟨100⟩ Si substrates. The sputtering systems applied, deposition methods and resulting film morphologies and layer properties for both materials have been detailed elsewhere [3, 4, 11]. The refractive indices of the Al_2O_3 and Y_2O_3 layers were measured using a spectroscopic ellipsometer, and were found to be 1.65 ± 0.01 and 1.94 ± 0.01, respectively, at 633 nm. The thickness of the deposited films ranged from approximately 500 to 900 nm. To develop the Al_2O_3 and Y_2O_3 channel waveguide fabrication process, various potential common mask materials were investigated in terms of patterning methods, etch selectivity and possible removal after etching. Accordingly, 3-μm-thick plasma-enhanced chemical vapour deposited (PECVD) SiO_2 and Si_3N_4 films, standard 1.5-μm photoresist films and 200-nm-thick electron-beam-evaporated Ni and Cr layers were also prepared on Si substrates.

The etch experiments were carried out using an Oxford Plasmalab 100 inductively coupled plasma (ICP) RIE system. The system was designed for 100-mm wafers, which were introduced to the chamber through a load-lock and fixed on a substrate holder with a water-cooled electrode. The ICP source was controlled by a 3-kW, 13.56-MHz rf generator, while substrate bias was controlled separately by a 600-W, 13.56-MHz rf generator. Various standard process gases and combinations of these gases were used, including BCl_3, BCl_3/HBr (50 : 50), CF_4/O_2 (90 : 10), Cl_2, Cl_2/Ar and Ar. In preliminary Y_2O_3 etching experiments, the etch rate was found to be relatively independent of gas flow, and to increase with decreasing chamber pressure, increasing ICP power, and increasing rf substrate electrode power and self-bias. Therefore, in order to compare the etch rate in various gas chemistries, the total gas flow was held constant at 50 sccm (measured by mass flow control units), while the process pressure (measured by a capacitance manometer gauge) was maintained as low as possible, varying from 7–12 mTorr. Unless otherwise stated, the ICP power was held constant at 1500 W and the applied rf electrode power was varied from 100 to 400 W. The etch rates of the films were determined by measuring the film thickness before and after the etch process using a spectroscopic ellipsometer, while the etch rates of the Ni and Cr layers, patterned prior to etching by photolithography and wet chemical etching, were measured using a Dektak surface profilometer. Surface morphology was acquired using a Digital Instruments atomic force microscope (AFM). The processes developed for the fabrication of channel waveguides in Al_2O_3 and Y_2O_3 layers are discussed following the results of the etching experiments.

3 Reactive ion etching

In this section the etching behaviour of the Al_2O_3 and Y_2O_3 films in the various ICP RIE chemistries and their selectivity to potential mask materials will be discussed and compared.

3.1 Al_2O_3 *etching*

The etch rate of the Al_2O_3 films was investigated as a function of applied rf power for various plasma compositions. Figure 1 shows the measured etch rate of Al_2O_3 films as a function of rf power for CF_4/O_2 (90% : 10%), BCl_3 (100%), BCl_3/HBr (50% : 50%), Cl_2 (100%) and Ar (100%) gases. The process pressure (which was the lowest attainable under each of the plasma conditions) was measured to be 10–12 mTorr (CF_4/O_2), 9 mTorr (BCl_3), 9 mTorr (BCl_3/HBr), 7–8 mTorr (Cl_2) and 8 mTorr (Ar).

The highest etch rate, 257 nm/min, was measured for CF_4/O_2 at 400 W and the etching in CF_4/O_2 is the most strongly dependent on rf power, indicating that etching under these conditions also depends strongly on the energy of ions directed onto the substrate (it is strongly ion assisted). The potential F-based etch products are expected to have lower volatilities (based on higher melting and boiling points) than Cl-based products, which is consistent with the observed

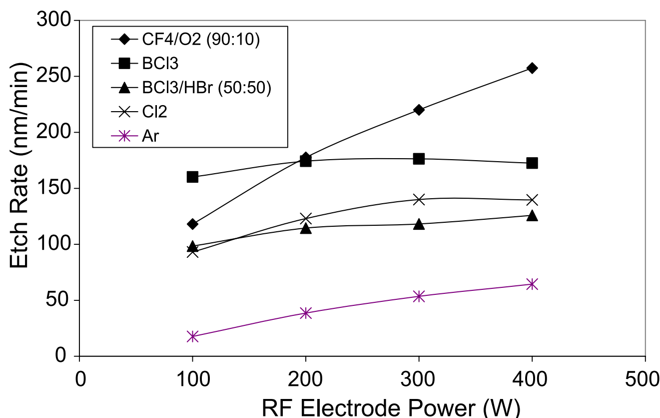

FIGURE 1 Etch rate as a function of rf power for Al_2O_3 films in $CF_4 : O_2$ (90% : 10%), BCl_3 (100%), $BCl_3 : HBr$ (50% : 50%), Cl_2 (100%) and Ar (100%) at a total flow rate of 50 sccm

stronger effect of ion energy on removing material from the surface and assisting the reaction. These data generally agree with the previous etching results for similar Al_2O_3 layers in CF_x gases [16]. The etching in Cl-containing gases is shown to be less dependent on rf power, indicating that chemical etching, rather than ion-assisted etching, more strongly affects the etch rate and behaviour. Of the Cl-containing gases, the etch rate is shown to be significantly higher in BCl_3 than Cl_2 or BCl_3/HBr (50% : 50%). In the case of all the halogen-based (Cl, F) processes, the etch rate is almost an order of magnitude higher than etching in Ar, which strongly indicates that an additional chemical component aids the etching process for Al_2O_3 in those cases.

3.2 Y_2O_3 *etching*

The etch rate was also measured as a function of rf power for the Y_2O_3 films for the same process gases, as shown in Fig. 2. The process pressures, which varied slightly compared with those measured for Al_2O_3 due to drift in the system performance, were 10–12 mTorr (CF_4/O_2), 9 mTorr (BCl_3), 9 mTorr (BCl_3/HBr), 7–8 mTorr (Cl_2) and 8 mTorr (Ar). From these results, it can be seen that with the exception of Ar, the various etch chemistries do not significantly impact the etch rate. Ar clearly exhibits the highest overall etch rates, with a maximum value of 127 nm/min observed at 400 W rf power.

In comparison to Al_2O_3, the Y_2O_3 etch rates are all much lower for the different process gases, except in the case of Ar (a non-reactive gas). The chemical volatility of the potential etch products (represented by their melting and boiling points) gives an indication of the expected etching behaviour. Table 1 gives the known melting and boiling points of various possible etch products of Al_2O_3 and Y_2O_3 in the F- and Cl-containing gases studied. The potential etch products of Y_2O_3 (such as YCl_3, YBr_3, YB_6) indeed have much higher melting points than the corresponding compounds containing Al (except in the case of AlF_3 where the sublimation point is given). Therefore, we expect potential Y_2O_3 etch products to be less volatile in general and the etch rates to be much lower than Al_2O_3, which is in agreement with the experimental results.

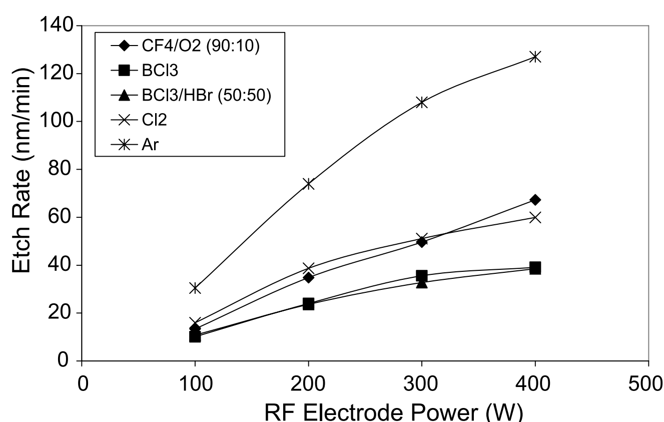

FIGURE 2 Etch rate as a function of rf power for Y_2O_3 films in $CF_4 : O_2$ (90% : 10%), BCl_3 (100%), $BCl_3 : HBr$ (50% : 50%), Cl_2 (100%) and Ar (100%) at a total flow rate of 50 sccm

The similar etch rate curves of Y_2O_3, combined with the lower etch rates in the Cl- and F- based gases than those observed in Ar, are strong evidence that physical etching (sputtering) dominates for all the process gases. Ar is a non-reactive noble gas, which means that Ar ions reaching the substrate only contribute to the etch process through physical breaking of the highly stable Y-O bonds. Non-identical process conditions coupled with the differing atomic weights and size of the bombarding species between the various process gases may explain the higher etch rates observed in Ar. In particular, the process pressure, which was found to have an inverse relationship with the etch rate, was 2 to 4 mTorr higher in the case of CF_4/O_2 compared with Ar. However, chlorine has a similar atomic weight to argon and the process pressure in the case of Cl_2 was actually lower than Ar. The lower etch rates in Cl_2 can be explained by investigating in more detail the reactive ion etching mechanisms at the surface for each process gas.

The surface quality of the etched Y_2O_3 films varied significantly depending on the process gas. The variation in surface quality was indicated by the quality of the ellipsometric fit. After etching in BCl_3, BCl_3/HBr and Cl_2 the quality of the fit became much poorer (indicated by the mean square error), while for CF_4/O_2 and Ar the quality remained relatively the

Al_2O_3			Y_2O_3		
Etch product	Melting point (°C)	Boiling point (°C)	Etch product	Melting point (°C)	Boiling point (°C)
AlB_2	> 920	–	YB_6	2600	–
Al_4C_3	2100	> 2200	YC_2	∼ 2400	–
$AlBr_3$	97.5	255	YBr_3	904	–
$AlCl_3$	192.6	180 (s)	YCl_3	721	–
AlF_3	∼ 2250 (t)	1276 (s)	YF_3	∼ 1150	–
Al_2O_3	2053	∼ 3000	Y_2O_3	2438	–
Al	660.32	2519	Y	1522	3345
$Al(BH_4)_3$	– 64.5	44.5	–		
AlH_3	> 150	–	–		
H_2O	0	100			
O_2	– 218.4	– 182.9			

s = sublimation point, t = triple point

TABLE 1 Melting and boiling points of possible etch products of Al_2O_3 and Y_2O_3 [25]

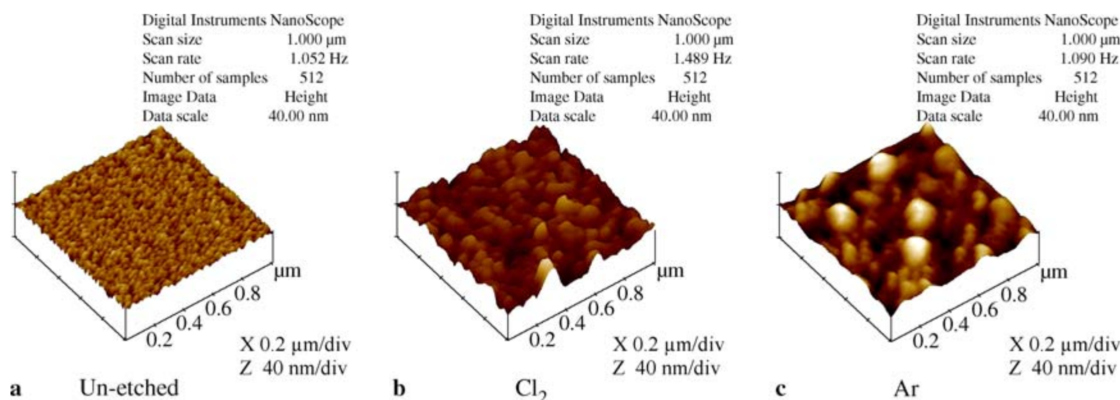

FIGURE 3 AFM 3D surface plots for a Y_2O_3 film (**a**) before etching and (**b**) and (**c**) after etching in Cl_2 and Ar plasma, respectively, with 400 W rf power applied

same. It was found that the quality of the fit could be improved by using a so-called effective-medium approximation (EMA) to approximate an additional thin layer at the surface. The EMA method can be used to measure a film with a rough surface by approximating the rough portion of the film with an additional layer composed of a mixture of the film material itself and a certain percentage of void space in the film. Including this EMA layer for films etched in Cl_2, BCl_3 and BCl_3/HBr greatly improved the fit, while it affected the already good fit of the Ar- and CF_4/O_2-etched films very little. In order to verify these results, surface measurements were obtained using AFM for an un-etched sample, a sample etched in Cl_2 and a sample etched in Ar. After etching at an applied power of 400 W in Cl_2, the EMA fit gave a surface layer thickness on the order of 45 nm. Surface morphology and particle (or grain) size analysis using AFM are shown in Fig. 3. In Fig. 3a, the un-etched film shows good uniformity and relatively small particle size, with an average particle height on the order of 10 nm. In Fig. 3b, the surface uniformity of the Cl-etched film is clearly poorer, and the average particle height is 47 nm, which agrees with the EMA measurements. In Fig. 3c, the Ar-etched film, although appearing to have some larger features than the un-etched sample (perhaps due to micro-masking), has an average particle size of 23 nm, approximately half the size of the Cl-etched film. For the Al_2O_3 films, etching in all process gases resulted in a good ellipsometric fit (similar to the un-etched films), therefore indicating good surface quality.

Thermodynamic equilibrium calculations [26] (which can only give an indication of etching behaviour under non-equilibrium plasma conditions) for Cl_2 and Y_2O_3 for pressures in the range of 1 to 200 mTorr and temperatures in the range of -25 to 250 °C predict some formation of YCl_3 as well as O_2. In [22], measurements also confirmed the formation of YCl_3 during etching. Similar calculations predict the formation of mainly YCl_3 and B_2O_3 in BCl_3 and HBr, and no reaction with CF_4/O_2 or Ar. Therefore, the additional layer observed on the surface of the Y_2O_3 films could in fact be explained by formation of a non-volatile etch product such as YCl_3. To further support the conclusion of YCl_3 forming on the surface, the samples were rinsed in deionized water, which YCl_3 is known to be soluble in, and re-measured, and the fit was greatly improved, indicating that the surface layer had been partially or entirely removed. During etching, the formation of YCl_3 on the surface could act as an etch-blocking layer, explaining the lower etch rates observed in Cl-containing gases (and the much higher etch rate observed in Ar under similar conditions).

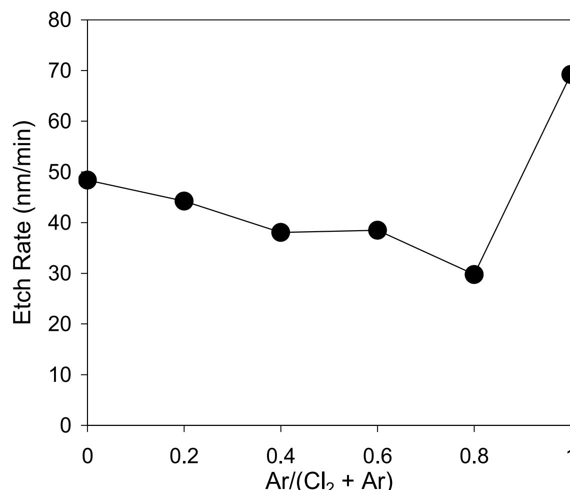

FIGURE 4 Etch rate of Y_2O_3 as a function of Ar to Cl_2 ratio, with a constant total gas flow rate of 50 sccm and a constant applied rf power of 300 W

In order to investigate if an increased physical etching component could help remove blocking non-volatile etch products from the surface during Cl_2 etching, a mixture of Cl_2 and Ar was used. Figure 4 shows the etch rate as a function of Cl_2/Ar mixing ratio. As the Ar content was increased, the etch rate in fact decreased, until an abrupt increase was observed at 100% Ar content. Furthermore, the fitted EMA surface layer thickness was found to be similarly high in all cases, except in the case of 100% Ar where it was negligible. Therefore, increased Ar content in a Cl/Ar mixture was found to provide no enhancement to the etch rate, giving further evidence that the non-volatile layer contributes to etch blocking. At 100% Ar the etch rate increases dramatically and the EMA surface layer thickness becomes negligible, indicating that the etch-blocking effect is removed. In addition, the pressure, ICP power and gas flow were varied over a wide range for 100% Cl_2; however, no process window could be found whereby the blocking layer became volatile and the etch rates significantly increased. Thus, unlike the case of Al_2O_3 where chemical re-

Material	CF_4/O_2 (90 : 10)	BCl_3	Process gas BCl_3/HBr (50 : 50)	Cl_2	Ar
Photoresist	< 0.20	0.67	0.54	0.16	0.57
PECVD SiO_2	0.60	0.95	0.80	0.70	0.35
PECVD Si_3N_4	0.35	1.35	1.80	0.65	0.45
Silicon	0.39	0.98	2.15	0.30	0.25
Nickel	5.82	–	3.51	1.38	0.27
Chromium	–	–	–	< 0.94	–

TABLE 2 Maximum selectivities of Al_2O_3 to possible mask materials, for various process chemistries, at a total gas flow rate of 50 sccm, ICP power of 1500 W, varying rf electrode power (100 to 400 W) and process pressure in the range of 6 to 14 mTorr

Material	CF_4/O_2 (90 : 10)	BCl_3	Process gas BCl_3/HBr (50 : 50)	Cl_2	Ar
Photoresist	< 0.03	0.05	0.03	0.03	0.81
PECVD SiO_2	0.15	0.20	0.25	0.25	0.65
PECVD Si_3N_4	0.10	0.20	0.25	0.15	0.90
Silicon	0.09	0.06	0.44	0.11	0.43
Al_2O_3	0.30	0.25	0.35	0.45	2.05
Nickel	1.31	–	0.59	0.50	0.46
Chromium	–	–	–	< 0.30	–

TABLE 3 Maximum selectivities of Y_2O_3 to possible mask materials, for various process chemistries, at a total gas flow rate of 50 sccm, ICP power of 1500 W, varying rf electrode power (100 to 400 W) and process pressure in the range of 6 to 14 mTorr

activity and volatile etch products in F- and Cl-based process gases significantly enhance the etch rate (compared to purely physical etching), the observed reactivity of Y_2O_3 in Cl_2 cannot be used to enhance the overall etch rate.

3.3 *Etching of mask materials*

The etch rates of several common mask materials, chosen for structuring Al_2O_3 and Y_2O_3 mainly because these mask materials can be easily deposited and patterned in our laboratory, were also measured. The principal requirements for a good mask material are that it can be easily patterned, it has a high selectivity compared to the material to be etched (for good pattern transfer and high resolution) and it must be possible to selectively remove the mask material from the substrate after etching. Generally, selectivities much greater than 1 are preferred; however, for the more highly stable dielectric materials Al_2O_3 and Y_2O_3 we expect lower selectivities. Tables 2 and 3 show the maximum selectivities measured for Al_2O_3 and Y_2O_3 to the various prospective mask materials, respectively. The process window used to determine the mask material etch rates was essentially the same as that used for the Al_2O_3 and Y_2O_3 etching experiments (ICP power = 1500 W, rf electrode power = 100 to 400 W, pressure = 6 to 14 mTorr, total gas flow = 50 sccm). The selectivity in general was found to be two times lower for patterned as opposed to un-patterned mask layers.

Overall, the selectivities were much higher for Al_2O_3 than Y_2O_3, as follows from the higher etch rates of Al_2O_3. For all mask materials except Ni, the selectivity versus Al_2O_3 was generally higher in BCl_3 and BCl_3/HBr. The selectivities for Si_3N_4 were > 1 for these gases; however, selective removal of Si_3N_4 from the Al_2O_3 layer after etching was found to be a problem. The selectivities to Ni are also quite high in comparison to other materials, as we would expect for a harder metal mask; however, if possible it is better to avoid metal masks for optical applications, as any residual metal remaining after etching and the mask removal can introduce additional optical losses. For Cr, significant data is missing because it was realized early in the experiments that patterning mask layers with smooth sidewalls was difficult – perhaps due to the layer deposition process or quality of the Cr films. Furthermore, the etch rates were generally higher for Cr than for Ni, so Cr was ruled out as a possible mask material. Therefore, for reasons of simplicity, it was decided to use photoresist as a mask, varying the parameters to improve the selectivity and using the BCl_3/HBr system because this gave the highest overall selectivities.

For Y_2O_3, the selectivities were much poorer because of the lower etch rates. Apart from a value of 1.31 for Ni in CF_4/O_2, the only selectivities close to or greater than 1 were in Ar, where values of 0.81, 0.90 and 2.05 were measured for photoresist, Si_3N_4 and Al_2O_3, respectively. Ni had the additional problem that the wet etching solution used to remove the Ni layer after etching also strongly etched the Y_2O_3 layer itself. Both metal layers (Ni and Cr) were found to react with the Cl-containing gases (also predicted by thermodynamic equilibrium calculations), leaving residue on the surface. Although some chemical etching is preferred, due to the poor selectivities, the blocking layer in Cl_2, BCl_3 and BCl_3/HBr, and primarily overall physical etching of Y_2O_3, it was decided to use Ar as a process gas, with either standard resist as a mask due to its straightforwardness, or Al_2O_3 as the mask material due to its superior selectivity compared to the other materials.

4 Channel waveguide fabrication

4.1 Al_2O_3 *channel waveguides*

Al_2O_3 channel waveguides ranging from 1.2 to 8.0 μm in width were fabricated using a BCl_3/HBr gas mixture and a 1.5-μm photoresist mask layer patterned by standard lithography. These process gases have previously been demonstrated as a suitable gas mixture for etching straight, vertical ridge structures with smooth sidewalls in sapphire (crystalline Al_2O_3) [27, 28], with channel waveguides being demonstrated in Ti:sapphire layers using a BCl_3/Cl_2 mixture [29] (similar structures were also obtained by Ar-ion-beam milling [30] and have later been demonstrated to lase [31]). The optimized gas ratio in terms of selectivity for the amorphous Al_2O_3 films was found to be 5 : 2 (BCl_3:HBr) and optimized process parameters were ICP power = 1750 W, rf electrode power = 25 W, pressure = 12 mTorr and a total gas flow of 35 sccm. Figure 5 shows a side profile and a cross section of the resulting Al_2O_3 channel waveguide, demonstrating a width down to 1.3 μm. The etch depth was determined to be 530 nm (the thickness of the Al_2O_3 layer), while the etch rate was 59 nm/min and the selectivity to the resist mask was 0.76 (which is higher than the 0.54 in Table 2 because of lower applied rf electrode power). This film thickness and etch depth in such an Al_2O_3 layer are sufficient for single-mode channel wave-

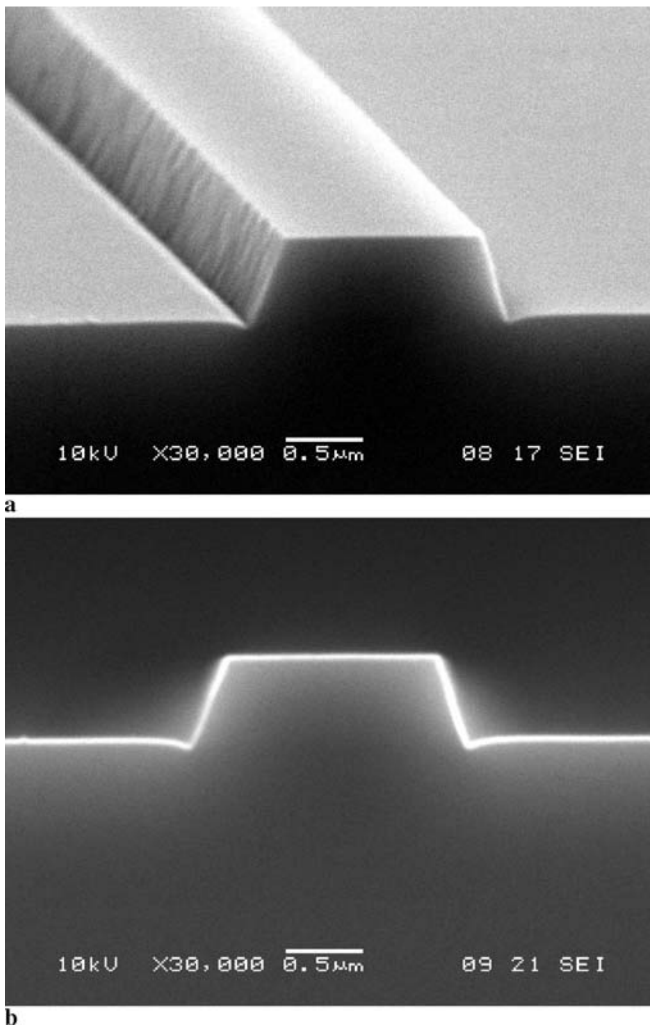

FIGURE 5 SEM micrograph of (**a**) profile and (**b**) cross section of a 1.3-μm-wide and 530-nm-deep channel waveguide in Al_2O_3

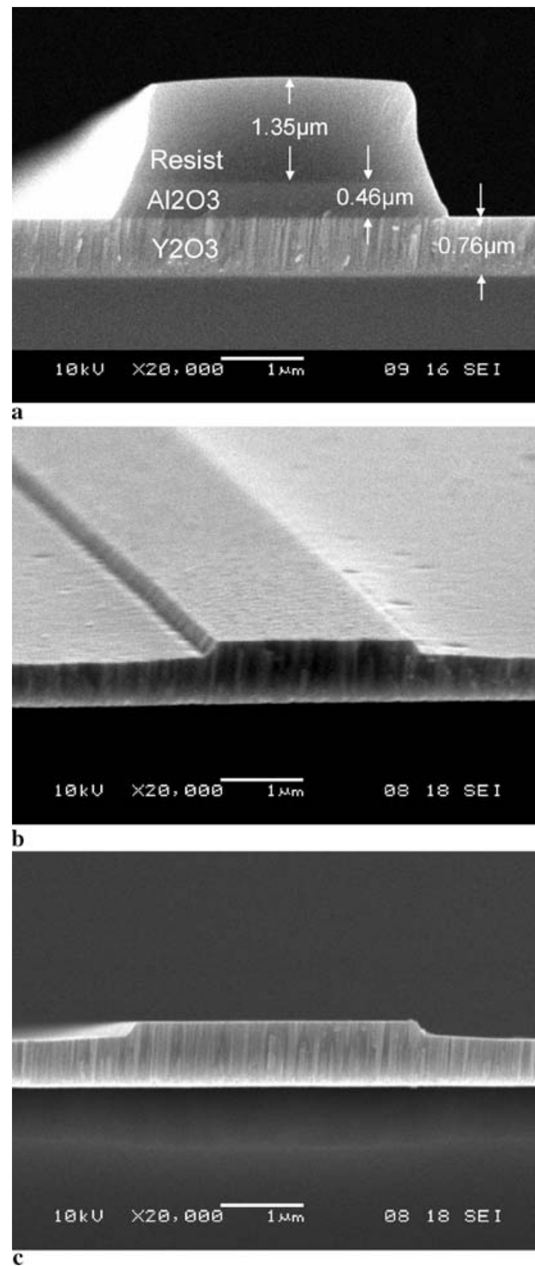

FIGURE 6 SEM micrographs of (**a**) a photoresist-patterned Al_2O_3 mask on Y_2O_3, (**b**) the resulting approximately 2.4-μm-wide, 250-nm-deep Ar-etched Y_2O_3 channel waveguide and (**c**) the cross section of a 3.4-μm-wide, 250-nm-deep Y_2O_3 waveguide on the same sample

guides up to 3-μm wide at wavelengths around 1550 nm. The channel sidewall angle ranged from 56° to 68° depending on the waveguide width and a slight trench was observed beside the waveguide, typical of RIE processes. The sidewall roughness in the picture can be attributed to pattern transfer from the mask layer itself. Such roughness could be decreased with the use of an E-beam (as opposed to a laser-lithography written) mask for the lithographic mask-patterning step.

4.2 Y_2O_3 *channel waveguides*

For Y_2O_3 channel waveguides, photoresist was used as a mask layer as well and the layers were etched in Ar at varying rf powers. For shallow etch depths the results were found to be sufficient (see optical measurements discussed further in this section). However, for larger etch depths, it was found that degradation of the mask layer due to the high rf powers and the long etching times required led to increased roughness of the sidewalls and deep trenches beside the Y_2O_3 waveguides, which would significantly add to the optical propagation losses. Therefore, as discussed above, due to its higher selectivity (selectivity ~ 2) in Ar, it was decided to use Al_2O_3 as a mask layer for Y_2O_3 as an alternative. A ~ 460-nm-thick Al_2O_3 layer was sputtered at 200 °C on a Si wafer containing a Y_2O_3 film. The Al_2O_3 layer was then patterned using the same lithography and BCl_3/HBr etch process discussed above and the results are shown in the cross section in Fig. 6a. The sample was then etched in Ar at an applied rf power of 100 W to a depth of 250 nm at a Y_2O_3 etch rate of 29 nm/min and a selectivity of 1.55, and the Al_2O_3 mask layer was removed, as shown in Fig. 6b and c. The sidewall profile and angle matched those of the Al_2O_3 mask layer, and the sidewall quality was not strongly influenced by the columnar polycrystalline structure of the Y_2O_3 layer, which is visible in the cross section scanning electron microscope

(SEM) images shown in Fig. 6. Waveguides ranging from 1.4-μm to 8.0-μm wide were successfully patterned in the Y_2O_3 layer. Due to the small influence of the polycrystalline structure on the sidewall profile, it is proposed that the etch process described here could also be applied to purely crystalline Y_2O_3 films, which offer the advantage of even higher absorption and emission cross sections when doped with rare-earth ions [32].

4.3 *Optical waveguide characterization*

In order to test the additional losses introduced by channel etching, single-mode ridge waveguide structures were patterned in low-loss Al_2O_3 and Y_2O_3 layers. For Al_2O_3, waveguides were defined using the optimized recipe, to an etch depth of 220 nm in a 740-nm-thick film. The etch-depth uniformity over the substrate was found to be $\pm 10\%$. Prior to etching, the optical losses of the film were measured to be 0.12 ± 0.02 dB/cm at a wavelength of 1523 nm using the prism coupling method. The optical losses of 2.5-μm-wide ridge waveguides, designed to be single mode at wavelengths around 1550 nm, were investigated using a fibre butt-coupling setup and a broadband erbium-doped fibre amplifier (1520–1580 nm) source. Using the cut-back method, with waveguide lengths of 5.65, 4.0, and 1.65 cm, a propagation loss of 0.21 ± 0.05 dB/cm was measured. This indicates that only small additional losses on the order of 0.1 dB/cm, such as scattering losses caused by sidewall roughness, are introduced by the dry-etching process.

Single-mode ridge waveguides were also fabricated in a 850-nm-thick Y_2O_3 layer with initial slab losses of 1.11 ± 0.17 dB/cm at 1523 nm, to an etch depth of 45 nm using Ar etching and a resist mask. The same setup as the one described above and the cut-back method, with varying waveguide lengths of 2.88, 1.85 and 1.00 cm, were also applied to measure the propagation losses in the Y_2O_3 waveguides. For four different waveguide widths ranging from 1.4–2.0 μm, average propagation losses of 1.14 ± 0.09 dB/cm were measured, demonstrating that the etching introduces very little additional loss. The results of such shallow-etched channels are promising, and further optical measurements will characterize the losses of higher-confinement, deeply etched channel waveguides in both materials.

5 Summary

The etch behaviour of amorphous Al_2O_3 and polycrystalline Y_2O_3 films has been investigated and compared. The Al_2O_3 films have much higher etch rates in all chemistries, except Ar, indicating a much stronger chemical component to the etching process. Sputter etching due to ion bombardment was determined to be the dominant etch mechanism for the Y_2O_3 films, although in chlorine-containing plasmas (Cl_2, BCl_3), chemical reactions at the surface appear to result in a non-volatile etch-blocking layer.

The etching results were used to fabricate channel waveguides in Al_2O_3 and Y_2O_3. In Al_2O_3, waveguides were fabricated using BCl_3–HBr plasma, resulting in sufficiently steep sidewalls with good surface quality. In Y_2O_3, due to the lack of strong chemical etching, Ar sputtering was used (also because Ar gave the highest etch rates) and resist and Al_2O_3 were used as mask layers. For shallow etch depths, a resist mask was found to be sufficient, while, for larger etch depths, an Al_2O_3 mask resulted in much improved sidewalls and little degradation of the mask material, allowing good resolution and etch depths of ≥ 250 nm, much higher than previously shown in Y_2O_3. The optical loss at 1550 nm was measured for single-mode ridge waveguide structures in each material and it was found that both channel fabrication techniques introduce only small additional losses. Negligible additional losses were measured in shallow-etched Y_2O_3 waveguides and very low additional losses on the order of 0.1 dB/cm were measured in more deeply etched Al_2O_3 waveguides. The processes developed in this work will be used in the fabrication of active integrated optical devices in rare-earth-ion-doped Y_2O_3 and Al_2O_3 layers.

ACKNOWLEDGEMENTS The authors would like to acknowledge Peter Linders and Eddy Ruiter for their assistance with the etching experiments and AFM measurements, respectively. They would also like to thank Oxford Plasmalab Systems for their technical support. This work was primarily supported by funding through the European Union's Sixth Framework Programme (Specific Targeted Research Project 'PI-OXIDE', Contract No. 017501).

REFERENCES

1 A. Polman, J. Appl. Phys. **82**, 1 (1997)
2 G.N. van den Hoven, E. Snoeks, A. Polman, J.W.M. van Uffelen, Y.S. Oei, M.K. Smit, Appl. Phys. Lett. **62**, 3065 (1993)
3 T.H. Hoekstra, P.V. Lambeck, H. Albers, T.J.A. Popma, Electron. Lett. **29**, 581 (1993)
4 S. Musa, H.J. van Weerden, T.H. Yau, P.V. Lambeck, IEEE J. Quantum Electron. **QE-36**, 1089 (2000)
5 A. Suarez-Garcia, R. Serna, M. Jimenez de Castro, C.N. Afonso, I. Vickridge, Appl. Phys. Lett. **84**, 2151 (2004)
6 C.E. Chryssou, A.J. Kenyon, T.M. Smeeton, C.J. Humphreys, D.E. Hole, Appl. Phys. Lett. **85**, 5200 (2004)
7 O. Pons-Y-Moll, J. Perdiere, E. Million, R.M. Defourneau, D. Defourneau, B. Vincent, A. Essahiaoui, A. Boudrioua, J. Appl. Phys. **92**, 4885 (2002)
8 S. Bär, G. Huber, J. Gonzalo, A. Perea, M. Munz, Appl. Phys. A **80**, 209 (2005)
9 A.O.G. Dikovska, P.A. Atanasov, M. Jiménez de Castro, A. Perea, J. Gonzalo, C.N. Afonso, J. Garcia López, Thin Solid Films **500**, 336 (2006)
10 M.B. Korzenski, P. Lecoeur, B. Mercey, P. Carny, J.L. Doualan, Appl. Phys. Lett. **78**, 1210 (2001)
11 K. Wörhoff, J.D.B. Bradley, F. Ay, M. Pollnau, in *Conference on Lasers and Electro-Optics, Technical Digest 2007* (Optical Society of America, Washington, DC, 2007), paper CMW5
12 G.N. van den Hoven, R.J.I.M. Koper, A. Polman, C. van Dam, J.W.M. van Uffelen, M.K. Smit, Appl. Phys. Lett. **68**, 1886 (1996)
13 K. Solehmainen, M. Kapulainen, P. Heimala, K. Polamo, IEEE Photon. Technol. Lett. **16**, 194 (2004)
14 T.H. Hoekstra, *Erbium-Doped* Y_2O_3 *Integrated Optical Amplifiers* (University of Twente, Enschede, 1994)
15 B.J.H. Stadler, M. Oliver, J. Appl. Phys. **84**, 93 (1998)
16 W.G.M. Van den Hoek, Mater. Res. Soc. Symp. Proc. **68**, 71 (1986)
17 Y.H. Lee, Z.H. Zhou, D.A. Danner, P.M. Fryer, J.M. Harper, J. Appl. Phys. **68**, 5329 (1990)
18 J.W. Kim, Y.C. Kim, W.J. Lee, J. Appl. Phys. **78**, 2045 (1995)
19 J.W. Lee, B. Pathangey, M.R. Davidson, P.H. Holloway, E.S. Lambers, B. Davydov, T.J. Anderson, S.J. Pearton, J. Vac. Sci. Technol. A **16**, 2177 (1998)
20 D.P. Kim, J.W. Yeo, C.I. Kim, Thin Solid Films **459**, 122 (2004)
21 S. Tegen, P. Moll, J. Electrochem. Soc. **152**, G271 (2005)
22 Y.C. Kim, C.I. Kim, J. Vac. Sci. Technol. A **19**, 2676 (2001)
23 S.I. Shim, Y.S. Kwon, S.I. Kim, Y.T. Kim, J.H. Park, Solid-State Electron. **49**, 497 (2005)
24 E. van der Drift, B.A.C. Rousseeuw, J. Romijn, E.C.M. Pennings, F.H. Groen, Microelectron. Eng. **9**, 499 (1989)

25 D.R. Lide (ed.), *CRC Handbook of Chemistry and Physics*, 82nd edn. (CRC, Boca Raton, FL, 2001)
26 B.S. Bokstein, M.I. Mendelev, D.J. Srolovitz, *Thermodynamics and Kinetics in Materials Science: A Short Course* (Oxford University Press, Oxford, 2005)
27 C.H. Jeong, D.W. Kim, H.Y. Lee, H.S. Kim, Y.J. Sung, G.Y. Yeom, Surf. Coat. Technol. **171**, 280 (2003)
28 D.W. Kim, C.H. Jeong, K.N. Kim, H.Y. Lee, H.S. Kim, Y.J. Sung, G.Y. Yeom, Thin Solid Films **435**, 242 (2003)
29 A. Crunteanu, M. Pollnau, G. Jänchen, C. Hibert, P. Hoffmann, R.P. Salathe, R.W. Eason, C. Grivas, D.P. Shepherd, Appl. Phys. B **75**, 15 (2002)
30 C. Grivas, D.P. Shepherd, T.C. May-Smith, R.W. Eason, M. Pollnau, A. Crunteanu, M. Jelinek, IEEE J. Quantum Electron. **QE-39**, 501 (2003)
31 C. Grivas, D.P. Shepherd, T.C. May-Smith, R.W. Eason, M. Pollnau, Opt. Express **13**, 210 (2005)
32 S. Bär, H. Scheife, K. Petermann, G. Huber, Top. Appl. Phys. **106**, 401 (2007)